

Article

Investigation of Surface Modification of Bagasse Fibers: Performance of Asphalt Binders/Mixtures with Bagasse Fibers

Haiwei Xie ^{1,2,3}, Yixuan Jia ², Chunsheng Zhu ⁴, Weidong Liu ^{5,*}, Zuzhong Li ⁶ and Zhipeng Huang ⁶

¹ School of Traffic & Transportation Engineering, Changsha University of Science & Technology, Changsha 410114, China; xiehaiwei@xjau.edu.cn

² School of Traffic & Logistics Engineering, Xinjiang Agricultural University, Urumqi 830052, China; 320212702@xjau.edu.cn

³ Key Laboratory of Highway Engineering Technology and Transportation Industry in Arid Desert Regions, Urumqi 830000, China

⁴ Xinjiang Transportation Investment (Group) Co., Ltd., Urumqi 830000, China; zcsbest@163.com

⁵ Guangxi Key Laboratory of Road Structure and Materials, Guangxi Transportation Science and Technology Co., Ltd., Nanning 530007, China

⁶ School of Materials Science and Engineering, Chang'an University, Xi'an 710064, China; zuzhongli@chd.edu.cn (Z.L.); 2019902853@chd.edu.cn (Z.H.)

* Correspondence: liuwd2016@126.com

Abstract: The influence of surface modification on the properties of bagasse fibers and asphalt binders/mixtures was investigated. Bagasse fibers were modified by single, binary, and ternary methods with hydrochloric acid, sodium hydroxide, and sodium chlorite, respectively. The physical and chemical properties of bagasse fibers were analyzed by scanning electron microscopy, Fourier transform infrared spectroscopy, and an adsorption test, respectively. The rheological properties of asphalt binders with bagasse fibers or lignin fibers were analyzed by the dynamic shear rheometer test and bending beam rheometer test. In addition, the performance of asphalt mixtures with bagasse fibers or lignin fibers were evaluated by a wheel rutting test, bending test at a low temperature, and water stability test, respectively. In conclusion, the hydrophilic functional groups on the fiber surface were partially eliminated by modification, facilitating the degradation of different fiber components. Furthermore, the degree of fibrillation was improved, and more interfaces with asphalt components were formed, thus enhancing the high-temperature deformation resistance of asphalt binders, but slightly impairing its low-temperature performance. Among all modification methods, the ternary composite modification exerted important influences on fiber structure, oil absorption, and rheological properties of asphalt binders, significantly enhancing the performance of asphalt mixtures. Combined with surface modification methods, bagasse fibers would be promising reinforced pavement materials.

Keywords: bagasse fiber; surface modification; asphalt binder; properties



Citation: Xie, H.; Jia, Y.; Zhu, C.; Liu, W.; Li, Z.; Huang, Z. Investigation of Surface Modification of Bagasse Fibers: Performance of Asphalt Binders/Mixtures with Bagasse Fibers. *Buildings* **2024**, *14*, 1352. <https://doi.org/10.3390/buildings14051352>

Received: 13 April 2024

Revised: 26 April 2024

Accepted: 7 May 2024

Published: 9 May 2024



Copyright: © 2024 by the authors. Licensee MDPI, Basel, Switzerland. This article is an open access article distributed under the terms and conditions of the Creative Commons Attribution (CC BY) license (<https://creativecommons.org/licenses/by/4.0/>).

1. Introduction

The incorporation of biowaste enables the performance enhancement of asphalt at high and low temperatures, such as lignin waste, corn stover oil, and plant fibers, which have attracted widespread concerns for researchers [1–3]. A vast amount of bagasse, a by-product of the sugar industry, is generated annually in the world. A majority of the bagasse is disposed to produce electricity by incineration or stockpiling along landfill sites, which ultimately threatens the atmospheric quality and occupies land resources [4]. A growing aversion to pollution, together with concerns about the scarcity of resources, has motivated several countries to seek appropriate solutions regarding the utilization of sugarcane waste [5,6]. Except for biohydrogen production and ethanol production, bagasse has been mainly employed as a raw material for papermaking or prepared as fibers and then utilized in composite materials in recent years [7–11]. In addition, bagasse

has also been used in applications in the field of road engineering due to its low cost, high specific modulus, and acceptable mechanical properties [12]. It has been verified that bagasse fibers and hemp fibers can both be used in asphalt mixtures, which can enhance the resilient properties of the asphalt mixtures and effectively improve the rutting resistance of pavement [2,13]. Nonetheless, bagasse fibers, as the binder retainer in polymer matrix composites, has faced some notable problems that need to be solved urgently, such as high hygroscopicity, low thermal stability, and poor interfacial bonding with the matrix. Hence, it is necessary to further observe and improve the properties of bagasse fibers.

The interfacial adhesion between bagasse fibers and the polymer matrix plays a critical role in the properties of composites. Plant fibers are universally known to have strong hydrophilicity because of the quantities of hydroxyl groups on the surface, which leads to the incompatibility between the fibers and the hydrophobic polymer matrix [14]. Moreover, pectin and waxy substances on the surface of fibers can prevent the interface reaction between fibers and the matrix [15]. The incompatible interface affects the stress transfer of the polymer matrix to the fibers and reduces the performance of the composites [16]. Morphologically, the main components of bagasse are composed of 30–50% cellulose, 19–54% hemicellulose, and 15–35% lignin, which means poor compatibility with the polymer matrix, similar to other plant fibers [17]. Based on the above instances, it is vital to explore an appropriate treatment of bagasse fibers to fulfill its reinforcement effect in composites.

Currently, surface modification via chemical treatments is considered the most efficient strategy to promote the performance of plant fibers in composites. The popular methods involve alkalization, acetylation, benzoylation, silane treatment, coupling agent treatment, peroxide treatment, and isocyanate treatment, etc. [15]. Conium maculatum fiber has been treated with alkali, silane, potassium dichromate, potassium permanganate, and silicone oil. The hydrogen-bond intensity (HBI) and the O/C atomic ratio of the fibers increased after treatment, and the highest increment was achieved by alkali treatment [18]. Also, it was reported that fiber–matrix adhesion was promoted by fiber surface modifications, and better mechanical properties of hemp fiber-reinforced composites could be attained [19]. Cornstalk fibers treated by sodium hydroxide solution can be a substitute for lignin fibers in asphalt pavement [20]. Hence, combined with surface modification methods, plant fibers are widely used in composites owing to their advantages of being low-cost and environmentally friendly.

For demonstrating the modification mechanism and evaluating the effect of plant fibers in composite materials, several methods were extensively adopted to investigate the microstructure and chemical functional group of plant fibers as well as the performance of the composites [17,21–23]. In general, scanning electron microscopy (SEM) was conducted to observe the microstructure and the surface morphology of modified and un-modified plant fibers. Fourier transform infrared spectroscopy (FTIR) is widely used in cellulose research since it provides a relatively convenient approach to directly derive information about evolution during surface processing. In addition, an oil absorbing test was performed to examine the lipophilicity of fibers and evaluate the compatibility between fibers and the asphalt matrix [24–28]. Furthermore, a variety of methods, including a cone penetration test, dynamic shear rheometer (DSR) test, and bending beam rheometer (BBR) test, were tentatively proposed to characterize the rheological properties of asphalt with and without fibers at different temperature ranges [29–32].

This work was initiated with the objective to study the physical and chemical properties of bagasse fibers before and after surface treatments and to analyze the effect of bagasse fibers on the properties of asphalt binders/mixtures. All bagasse fibers were prepared by a series of processing methods, including soaking, high-speed centrifuge machining, drying, and screening. The prepared bagasse fibers were modified by single, binary, and ternary methods with hydrochloric acid, sodium hydroxide, and sodium chlorite, respectively. Subsequently, the microstructure and properties of untreated and treated bagasse fibers were explored by SEM, FTIR, and an adsorption test. The rheological properties of asphalt binders with bagasse fibers or lignin fibers were analyzed by the DSR and BBR tests.

Moreover, the reinforcement effects of bagasse fibers on asphalt mixtures were evaluated by a series of tests, including the wheel rutting test, bending test at a low temperature, and water stability test.

2. Materials and Methods

2.1. Materials

2.1.1. Preparation of Bagasse Fibers

The bagasse used in the present work was supplied by the sugarcane industry in Guangxi, China. The raw bagasse was cleaned to remove impurities and then soaked at room temperature for 20–24 h. Afterwards, the bagasse in a saturated state was splitted continuously at a shear rate of nearly 35,000 r/min in a high-speed multifunctional machine. Next, the bagasse was separated from the solid–liquid mixtures and dried to a certain moisture content. The bagasse fibers with an aspect ratio between 20 to 30 were collected for storage until use. A photograph of the original bagasse fibers is shown in Figure 1.



Figure 1. Photograph of original bagasse fibers.

2.1.2. Surface Modification

The prepared bagasse fibers were modified by single, binary, and ternary methods. As for single modification, a series of orthogonal tests with three factors and three levels, including proportion, temperature, and time, were conducted, and then, the best modified parameters were confirmed according to the change in the key index for their performance. Likewise, with regard to the binary composite modification and ternary composite modification, several schemes were also designed with different material compositions, and the optimal schemes were selected by comparing the effect of modification.

For single modification, the bagasse fibers were immersed in a chemical reagent at a preset temperature and then washed with distilled water to remove the residual reagent. For binary composite modification, the fibers were soaked in sodium chlorite for 80 min and then transferred to hydrochloric acid after cleaning. For ternary composite modification, the fibers were treated with sodium hydroxide, sodium chlorite, and hydrochloric acid sequentially. Each step was followed with one cleaning step. The detailed parameters of modification schemes for bagasse fibers are listed in Table 1. Lignin fibers were bought from the market and selected as a control product; they are widely used in asphalt pavement.

2.1.3. Preparation of Asphalt Binders with Fibers

The basic technical properties of SBS-modified asphalt (I-C) were tested according to the ASTM standards, listed in Table 2.

Table 1. The experimental conditions of the modification schemes.

| Method | Chemical Reagent | Proportion | Temperature | Time | Code Name |
|--------------------------------|---------------------|------------|-------------|------|-----------|
| | | % | °C | min | |
| Single modification | Hydrochloric acid | 1.5 | 60 | 100 | BF-2 |
| | Sodium hydroxide | 1.5 | 30 | 100 | BF-3 |
| | Sodium chlorite | 0.5 | 80 | 80 | BF-4 |
| Binary composite modification | Sodium chlorite | 0.5 | 80 | 80 | BF-5 |
| | + hydrochloric acid | 1.5 | 60 | 100 | |
| Ternary composite modification | Sodium hydroxide | 1.5 | 30 | 100 | BF-6 |
| | + sodium chlorite | 0.5 | 80 | 80 | |
| | + hydrochloric acid | 1.5 | 60 | 100 | |

The original bagasse fibers and lignin fibers were denominated as BF-1 and LF, respectively.

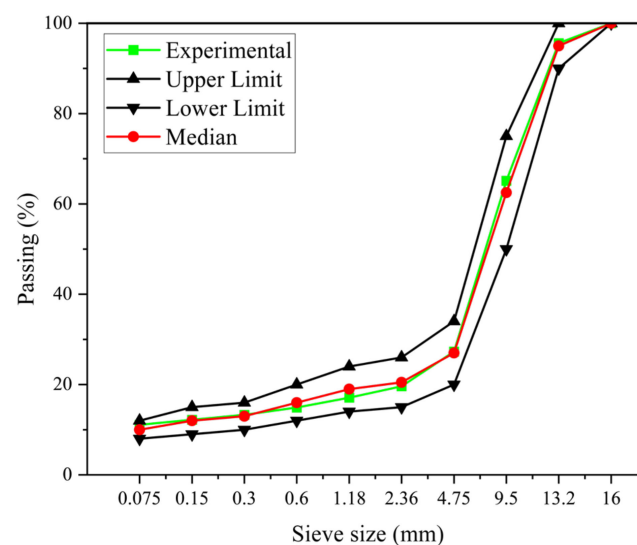
Table 2. The basic technical properties of SBS-modified asphalt (I-C).

| Tested Property | Units | Value | Standard [33] |
|-----------------------|--------|-------|---------------|
| Penetration (25 °C) | 0.1 mm | 69 | ASTM D5-13 |
| Softening point | °C | 82.5 | ASTM D36-76 |
| Ductility (5 °C) | cm | 48 | ASTM D113-99 |
| Viscosity (135 °C) | Pa·s | 2.2 | ASTM D2170 |
| Flash point | °C | 265 | ASTM D92 |
| Solubility | % | 99.4 | ASTM D2042 |
| Separation difference | °C | 1.0 | ASTM D5976 |

The fibers were blended with melted asphalt at 165 °C in batches until a homogeneous distribution was obtained. The blend quantity of the fibers was restricted at about 3% (relative to asphalt weight). These specimens were used for the laboratory tests for the rheological properties, as discussed later.

2.1.4. Preparation of Asphalt Mixtures with Fibers

To investigate the reinforcement effect of different modified bagasse fibers on asphalt mixtures, the mixtures of SMA-13 were employed with a fiber content of 0.3%, and an optimal oil–stone ratio of 6.0% was selected. In addition, lignin fibers were used as control groups. The gradation of mixtures is detailed in Figure 2. Furthermore, a series of tests on high-temperature stability, low-temperature crack resistance, and water stability were conducted to study the road performance of asphalt mixtures with bagasse fibers or lignin fibers.

**Figure 2.** Gradation chart of mixtures.

2.2. Methods

2.2.1. SEM Test

In this study, scanning electron microscopy (SEM) analysis was conducted to visualize the microstructure and fracture surfaces of bagasse fibers before and after the modification of its physical properties and adsorption capacity. Regarding the sample preparation, cement was used to fix the fibers to facilitate the observation of the cross-section. Electron micrographs of the samples at different amplifications were captured by a scanning electron microscope (S4800). The experiments were run with a SEM resolution of 3–4 nm, a high vacuum, and an electron beam accelerating potential of 3–5 kV.

2.2.2. FTIR Test

Various bagasse fibers were scanned by a FTIR spectrometer ranging from 4000 to 400 cm^{-1} . All spectra were collected with a 1 cm^{-1} wavenumber resolution after 32 continuous scans. To facilitate the analysis, lignin fibers were selected to compare with bagasse fibers.

2.2.3. Oil Absorbing Test

Plant fibers can absorb the light components of asphalt, such as aromatics and resins, to enhance the interfacial compatibility between fibers and the matrix phase and improve the viscosity of the asphalt binder. The high lipophilicity of fibers guarantees good compatibility between fibers and the asphalt. The oil absorbing test was applied to measure the oil absorption ratio of bagasse fibers before and after surface modification.

In accordance with JT/T 533-2020 [34], 5 g of the fibers was stirred with 100 g of kerosene in glass beakers for 15 min and then kept at room temperature for 5 min. After that, the mixtures of kerosene and the fibers were poured into the container, and the residual liquid was obtained after the automatic operation of the apparatus. The oil absorption ratio was calculated according to the corresponding formula.

2.2.4. Rheological Test

To simulate the general traffic situation under various loading times and ambient temperatures, the DSR tests were conducted in the forms of temperature sweeps and frequency sweeps, as specified in ASTM D7175-15 [35]. The temperature sweep tests were conducted at a frequency of 10 Hz and temperature range of 40 °C to 82 °C. The frequency sweep tests were conducted from 40 °C to 70 °C, with an increment of 6 °C. At each temperature, the frequency varied from 0.1 rad/s to 10.0 rad/s. The test was run in parallel plate geometry with a diameter of 25 mm, and the height of the sample was 1 mm. Several rheological parameters (i.e., complex modulus G^* , phase angle δ , and rutting factor $G^*/\sin \delta$) were collected for all the samples. The data from the frequency sweep tests of all the samples were plotted as master curves. The CAM model was selected to simulate the master curve and characterize the viscoelastic behavior of the asphalt, and it was defined as follows:

$$G^* = G_g \left[1 + \left(\frac{f_c}{f} \right)^k \right]^{-\frac{m_e}{k}}$$

$$R = \frac{\log 2}{v}$$

where G^* is the complex modulus, G_g is the glass complex modulus as $f \rightarrow \infty$, f_c is the frequency at the cross point, f is the reduced frequency, m_e and k are shape parameters of model, and R is the rheological index.

The BBR test was implemented to evaluate the anti-cracking ability of the asphalt binder according to ASTM D6648-08 [36]. The creep modulus (S) and the creep rate (m) at three temperatures (i.e., -12 °C, -18 °C, and -24 °C) were calculated on the basis of the deflection of the beam under constant loading. To simplify the expression, each group of asphalt binders is listed with a code name in Table 3.

Table 3. The code name of asphalt binders.

| Matrix | Reinforcement | Code Name |
|-----------------------------|---------------|-----------|
| SBS-modified asphalt binder | / | AB-0 |
| | Lignin fiber | AB-LF |
| | BF-1 | AB-BF-1 |
| | BF-2 | AB-BF-2 |
| | BF-3 | AB-BF-3 |
| | BF-4 | AB-BF-4 |
| | BF-5 | AB-BF-5 |
| | BF-6 | AB-BF-6 |

3. Results

3.1. SEM Analysis

The cross-sectional microstructures of all the bagasse fibers by SEM are displayed in Figure 3. The bagasse fibers were composed of several individual microfibrils with hollow structure, compactly arranged to form a bunched fiber, approximately cylindrical. In addition, the microfibrils are bound together by lignin and hemicellulose. It was clearly recognized that the image of BF-2 was almost identical to that of BF-1. A potential reason was that cellulose was wrapped in lignin and hemicellulose, obstructing the degradation of cellulose catalyzed by hydrochloric acid. Differing from BF-1 and BF-2, BF-3 exhibited a significant change in surface morphology, attributable to the pectin, lignin, and hemicellulose in the middle lamella being dissolved by sodium hydroxide to expose more porosity and surface area of the hidden cellulose. The variation contributed to promoting the fibrillation degree and the capacity to absorb light components (like aromatics and resins) in asphalt, which was validated in the following analysis. Conversely, BF-5 was not treated by sodium hydroxide but presented a looser structure. In this case, it can be speculated that hot water could damage the surface structure of fibers and weaken the supporting function of the cell wall with an extension of the treatment. In addition, the cross-section of BF-4 was similar to that of BF-3, and the original microfibrils rarely changed. As for BF-6, the rough surface was in a loose and flexible state, which demonstrated that the treatment with sodium hydroxide did not encounter any obstacle in the reaction with the latter two modifiers.

3.2. FTIR Analysis

The FTIR spectra recorded for bagasse fibers and lignin fibers are displayed in Figure 4 and illustrated in Table 4. All fibers presented the typical vibration bands of different chemical functional groups from lignin, hemicellulose, and cellulose. The intense and broad peak at 3333 cm^{-1} corresponds to O-H from complex vibrational stretching. The double peaks observed at 2914 and 2796 cm^{-1} are caused by C-H asymmetric and symmetric stretching vibrations, respectively, in methyl and methylene groups. The tiny peak at 1728 cm^{-1} could be assigned to the stretching vibration of conjugated and unconjugated carbonyl ($\text{C}=\text{O}$) groups, which mainly exist in hemicellulose and lignin. The three peaks at approximately 1602 , 1510 , and 1426 cm^{-1} represent the absorption bands of aromatic rings, mainly originating from the components of lignin. The peak attained at 1243 cm^{-1} is ascribed to the C-O stretching vibration of the acetyl ester group in hemicelluloses. The prominent peak observed at 1033 cm^{-1} is attributed to the stretching of the C-O-C group. The absorption peak near 557 cm^{-1} refers to O-H groups stretching outside of the plane.

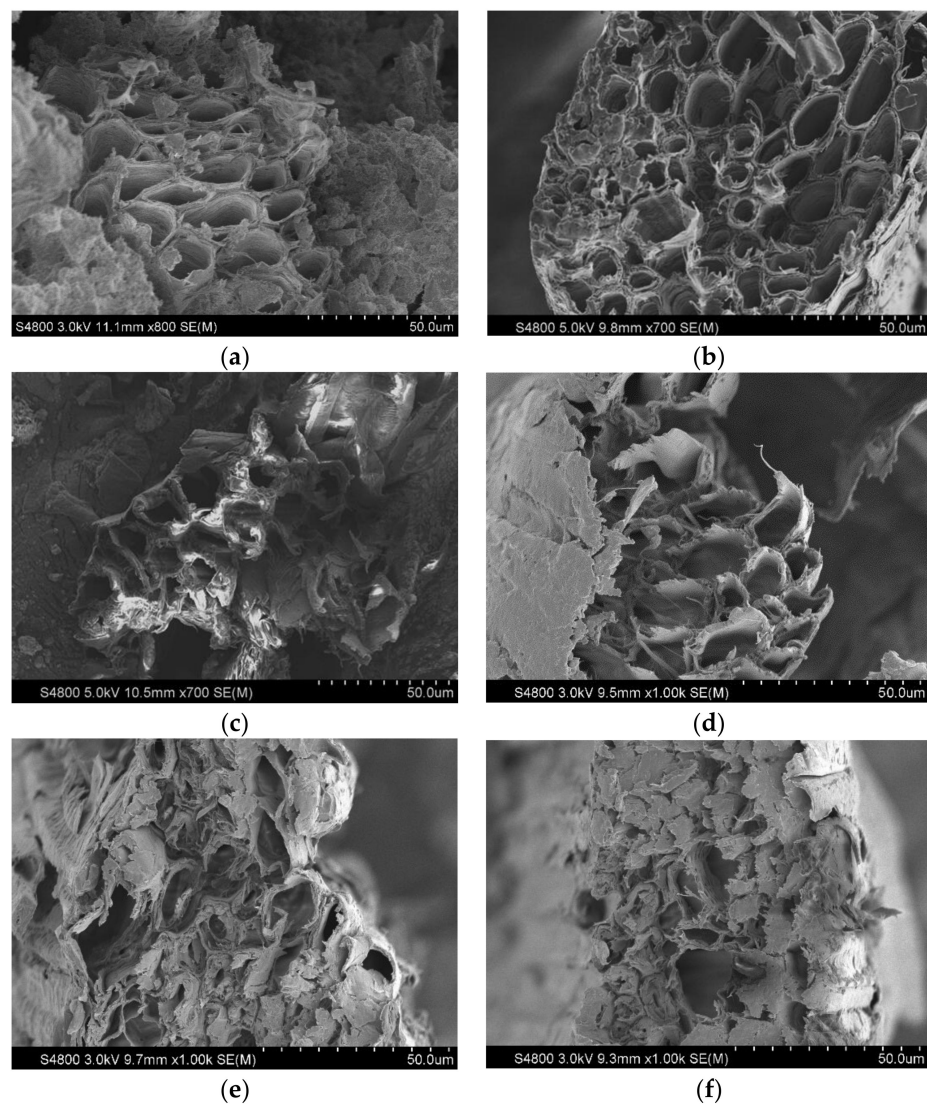


Figure 3. SEM images of bagasse fibers. (a) BF-1. (b) BF-2. (c) BF-3. (d) BF-4. (e) BF-5. (f) BF-6.

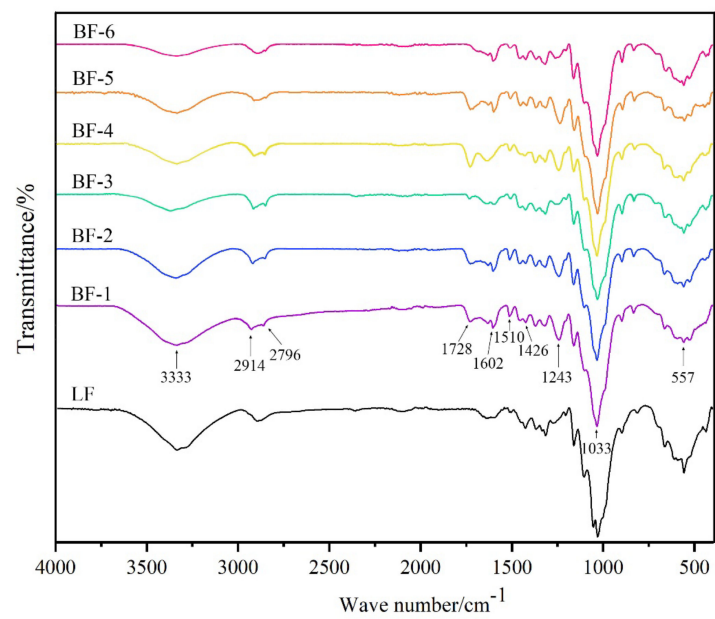


Figure 4. FTIR spectra of fibers.

Table 4. FTIR analysis peaks for lignin fibers and bagasse fibers.

| Wave Number (cm ⁻¹) | Functional Groups | Polymer |
|---------------------------------|-----------------------------------------------------------|--------------------------------------|
| 3333 | O-H from complex vibrational stretching | Cellulose |
| 2914–2796 | C-H asymmetric and symmetric stretching vibration | Lignin and hemicellulose |
| 1728 | Stretching vibration of carbonyl group (-C=O) | Hemicellulose and lignin |
| 1602 | Aromatic symmetrical vibration | Lignin |
| 1510 | C=C stretching of aromatic symmetrical vibration | Lignin |
| 1426 | C-H deformation (asymmetric) and aromatic ring stretching | Lignin |
| 1243 | C-O stretching vibration of acetyl ester group | Hemicellulose |
| 1033 | The stretching of the C–O–C group | Lignin, cellulose, and hemicellulose |
| 557 | O-H groups stretching outside of the plane | Cellulose and hemicellulose |

In Figure 4, it can be noticed that the intensity of the band at 3333 cm⁻¹ of five modified bagasse fibers was weakened in comparison to that of BF-1 for a different reason. With regard to BF-2, cellulose was degraded, and then, many monosaccharides were generated during the hydrochloric acid treatment. In the process of modification, the monosaccharide was dissolved in water so that the peak at 3333 cm⁻¹ subsided. The explanation involved BF-3 in a partial cleavage of hydroxyl by NaOH treatment. The intensity of the O-H stretching band corresponding to BF-4 also diminished for the oxidation of hydroxyl groups by sodium chlorite, translating into new products that appeared in low wavenumbers (1728 cm⁻¹). As for BF-5 and BF-6, the changes were jointly caused by the above reasons. The approximate absence of a peak at 1728 cm⁻¹ in BF-3 and BF-6 may be caused by the breakdown of the carbonyl group induced by hydrolysis, coupled with a disappearance of fatty acids on the fiber surface. Combined with the decrease in the absorption peak at 1510 cm⁻¹, it can be deduced that wax, hemicellulose, and lignin contents were partially degraded. Simultaneously, the C-O stretching of the acetyl ester group, presenting at 1243 cm⁻¹, confirmed a hydrolysis reaction of hemicellulose, mainly affected by sodium hydroxide. That is, the sodium hydroxide treatment triggered the presence of a cleaner cellulose phase with a high degree of polymerization because of a portion of lignin and hemicellulose being removed from the fiber surface, thus promoting the formation of a looser structure to facilitate the entry of light components in asphalt. In addition, the intensity changes in the bands at 2914, 2796, 1602, 1426, 1033, and 557 cm⁻¹ in all the groups were rather similar.

3.3. Oil Absorption Analysis

Table 5 shows the oil absorption ratio of the fibers, including lignin fibers. The results showed that the oil absorption ratio of the five modified fibers was greater than that of the original bagasse fibers. Compared to BF-1, the oil absorption ratio of BF-2 and BF-6 increased by 15.0% and 68.5%, respectively. After chemical modification, the surface of the fibers became looser and many hydrophilic reactive functional groups on the surface reacted together, similar to the findings of the SEM and FTIR analyses, which jointly improved the oil absorption of the fibers. It could be concluded that ternary composite modification and binary composite modification had the most significant effect on the oil absorption capacity of the bagasse fibers, followed by sodium hydroxide, sodium chlorite, and then hydrochloric acid.

Table 5. Oil absorption ratio results of bagasse fibers and lignin fibers.

| Fibers | LF | BF-1 | BF-2 | BF-3 | BF-4 | BF-5 | BF-6 |
|---------------------------------|-----|------|------|------|------|------|-------|
| Oil absorption ratio (multiple) | 6.4 | 6.20 | 7.13 | 8.83 | 8.16 | 9.89 | 10.45 |

3.4. Rheological Property Analysis

3.4.1. Temperature Sweep

To explore the influence of diverse modifications on the high-temperature stability of fiber-reinforced asphalt binders, the DSR test was conducted to obtain data on the complex modulus (G^*), phase angle (δ), and rutting factor ($G^*/\sin \delta$); the relationship curves between the rheological parameters of the asphalt binder and temperature are shown in Figures 5–7.

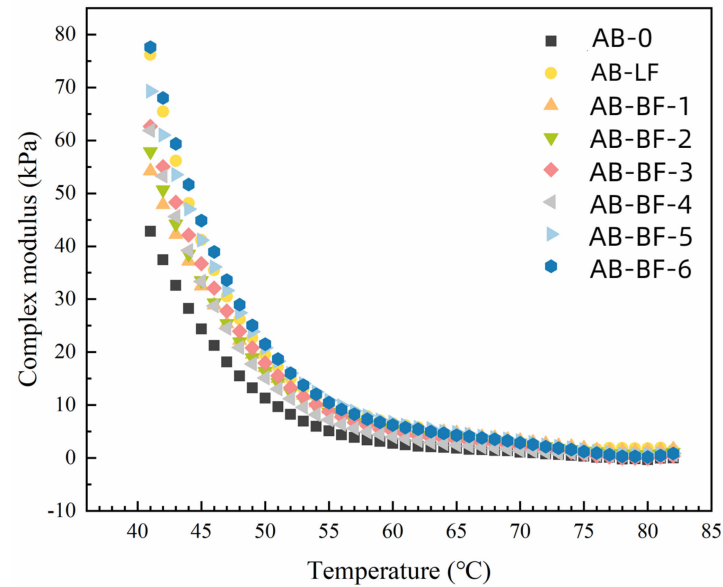


Figure 5. The complex modulus of asphalt binders based on the temperature sweep.

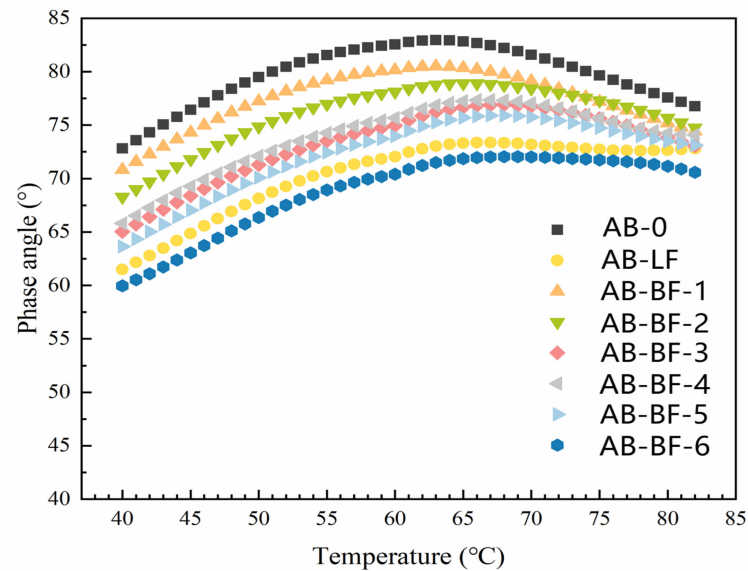


Figure 6. The phase angle of asphalt binders based on the temperature sweep.

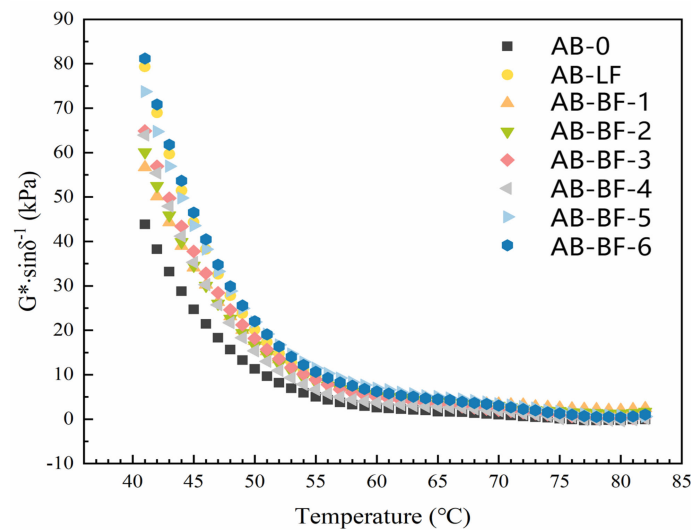


Figure 7. The rutting factor of asphalt binders based on the temperature sweep.

The complex modulus is defined as the ratio between stress and strain values and was chosen to reflect the stiffness of the asphalt. Figure 5 shows that the complex modulus was ever-dwindling and tended to approach a small value when the temperature increased in all cases. A reliable explanation is that the asphalt binder gradually softened as the temperature rose. When the test temperature reached a high level, the adsorption effect of the fibers on the asphalt was weakened, and the free portion in the asphalt binder increased such that the fibers could hardly reinforce the high-temperature stability of the asphalt. By contrasting AB-0 against the other groups, it was shown that the addition of fibers contributed to reducing the susceptibility of the polymer matrix to temperature, achieving higher stiffness, especially in intermediate temperature regions. The complex modulus of the asphalt with modified bagasse fibers, in comparison to AB-BF-1, grew by various extents. According to the relative position of the curve, the G^* of asphalt binders blended with treated bagasse fibers, ranked as follows: AB-BF-6 > AB-BF-5 > AB-BF-3 > AB-BF-4 > AB-BF-2. This was because the strong oil absorption of fibers endowed themselves with the ability to absorb asphalt components and consequently increased the stiffness of the asphalt. The surface treatment could further improve the oil absorption of bagasse fibers, as mentioned in the previous discussion. In addition, the lignin fibers used in this work possessed a high specific surface area, resulting in a better stabilization effect on asphalt as well as a strong interfacial combination between the fibers and the matrix, resulting in the curve of AB-LF being located above the one related to AB-BF-1.

The phase angle δ describes the ratio between the elastic and the viscous responses of the asphalt. The relationship curves between the phase angle and the test temperature for different asphalt binders with fibers are displayed in Figure 6. In all the groups, the δ had a moderate growth at the temperature range of 40–55 °C and, subsequently, a decrease at a temperature over 60 °C. The upward trend was caused by the transformation from an elastic component to a viscous component in asphalt, while the δ dropped at high-temperature regions on account of SBS copolymer phase domination. It was noticeable that the δ of the asphalt binder with fibers was lower than that of the pure SBS asphalt binder, indicating that the elastic portion of the asphalt binder was increased by the addition of fibers. This was mainly due to the high elastic modulus of fibers in accordance with the mechanical principle of the composites. In addition, the surface modification caused the fibers to be partially degraded so that the modified fibers had a larger specific surface area and aspect ratio. A large specific surface area provided more surface for the infiltration of light components in asphalt, relatively speaking, contributing to the decline in viscous composition and increase in elastic composition. As a result, AB-BF-6 possessed the smallest δ value at the same temperature.

Figure 7 shows the effect of treatment on the rutting factor ($G^*/\sin \delta$) with a change in the test temperature. Generally, a higher value of $G^*/\sin \delta$ indicates a better ability to resist deformation. From Figure 6, the rutting factor shows a decreasing trend with an increase in temperature. The order of $G^*/\sin \delta$ at the same temperature was $AB-BF-6 > AB-LF > AB-BF-5 > AB-BF-3 > AB-BF-4 > AB-BF-2 > AB-BF-1 > AB-0$, which was consistent with the sequence of the complex modulus. It was speculated that surface modification eliminated most impurities on the surface of the bagasse fibers, removed a portion of hydrophilic functional groups, and eroded the microfibrils to a certain degree. The structural evolution gave rise to the increase in specific surface area, which probably promoted the absorption of light components by bagasse fibers, together with forming a strong interface combination between the fibers and the asphalt matrix. Hence, the asphalt binders with modified bagasse fibers revealed better high-temperature stability.

3.4.2. Master Curve and CAM Model

The G^* master curves for all the groups at the reference temperature of 40 °C are presented in Figure 8. The larger complex modulus signified a better ability to resist rutting.

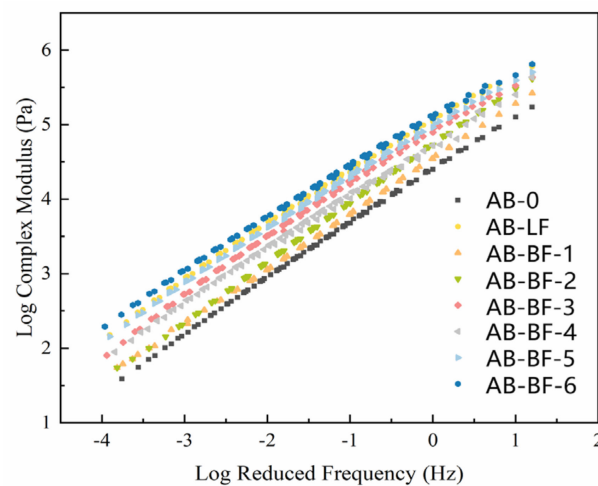


Figure 8. The G^* master curves of asphalt binders at the reference temperature of 40 °C.

The master curves of log frequency versus log complex modulus were approximately linear. The complex modulus of asphalt binders increased rapidly as the frequency increased. At a certain frequency, it was obvious that the variation trend of G^* was the same as the results of temperature sweep tests. More specifically, the order of G^* values was as follows: $AB-BF-6 > AB-LF > AB-BF-5 > AB-BF-3 > AB-BF-4 > AB-BF-2 > AB-BF-1 > AB-0$.

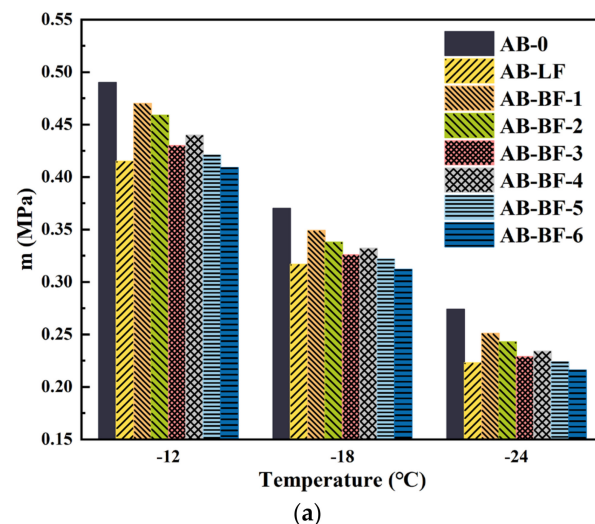
The CAM model points out a fit of the G^* results, and its parameters are shown in Table 6. The parameter m_e represents the slope of the third asymptote of the master curve. R , the rheological index, was calculated from the parameter k . The greater m_e and R were related to a stronger sensitivity to temperature and frequency variation. Based on this, $AB-BF-6$, $AB-LF$, $AB-BF-5$, and $AB-BF-3$ exhibited relatively greater performance. $AB-0$ and $AB-BF-1$ had an easy transition from the elastic part to the viscous part compared to the other binders. The conclusions were consistent with the results of temperature sweep tests and frequency sweep tests. The coefficients of determination R^2 were more than 0.995 and proved that the model could accurately present the actual viscoelastic behavior of asphalt binders.

Table 6. Results of fitting in CAM model.

| Sample | m_e | R | R^2 |
|---------|---------|--------|--------|
| AB-0 | 1.63063 | 0.9162 | 0.9995 |
| AB-LF | 1.34596 | 0.6023 | 0.9988 |
| AB-BF-1 | 1.66661 | 0.7916 | 0.9998 |
| AB-BF-2 | 1.53518 | 0.6581 | 0.9998 |
| AB-BF-3 | 1.34732 | 0.6161 | 0.9983 |
| AB-BF-4 | 1.56308 | 0.7311 | 0.9955 |
| AB-BF-5 | 1.35245 | 0.6211 | 0.9987 |
| AB-BF-6 | 1.30164 | 0.6007 | 0.9966 |

3.4.3. BBR

Figure 9 shows the creep rate and creep modulus of various asphalt binders at low temperatures in the BBR test. In Figure 9, all the laboratory specimens conformed to a common regularity, that is, the value of m decreased continuously, but the value of S grew gradually with the decrease in temperature. In the same graph, the indexes of each group had a similar sequence under different temperatures (i.e., AB-0, AB-BF-1, AB-BF-2, AB-BF-4, AB-BF-3, AB-BF-5, AB-LF, and AB-BF-6). Taking the bar graph at $-12\text{ }^\circ\text{C}$ in Figure 9a as an example, it was apparent that AB-BF-1 exceeded AB-LF with respect to the value of m , which signified that the crack resistance of the former, to a certain extent, was superior. This may be explained by the fact that the lignin fibers had undergone industrial treatment and assumed a cotton-shaped structure rather than that of a filament. On the one hand, the distribution density of lignin fibers in the asphalt was much greater than that of bagasse fibers. On the other hand, the lignin fibers with a cotton-shaped structure had a high specific surface area. These factors led to a high relative content of asphaltene in the specimens containing lignin fibers, indirectly weakening the low-temperature properties of the asphalt binder. Generally speaking, the incorporation of fibers was beneficial to the low-temperature properties of the asphalt binder, different from the conclusion of the BBR analysis. The explanation may lie in the adverse impact of non-uniform distributions and the ascendancy in oil absorption. The m value of the asphalt binder with different bagasse fibers depended on the oil absorption of the corresponding fibers. In other words, high oil absorption of bagasse fibers was conducive to accommodating more aromatics and resins and increased the asphaltene content, which exerted an adverse impact on the performance of the asphalt in a cold climate. This explained why the m value of the asphalt binder blended with various modified bagasse fibers was reduced at varying degrees. The discrepancy in the m value among experimental groups became narrow as the temperature dropped, while the difference in S expanded, which was attributed to the compound effect of the fibers and asphalt.

**Figure 9.** Cont.

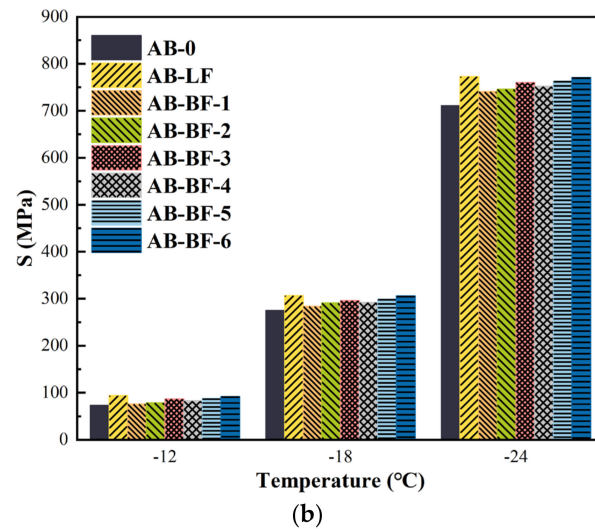


Figure 9. The creep rate (m) and the creep modulus (S) of asphalt binders. (a) The creep rate (m) of asphalt binders. (b) The creep modulus (S) of asphalt binders.

3.5. Performance of Asphalt Mixtures with Bagasse Fibers

To explore the influence of diverse modified fibers on the performance of the asphalt mixtures, a series of tests were conducted, including the wheel rutting test, bending test at a low temperature, and water stability test. The results of the tests are shown in Figures 10–12.

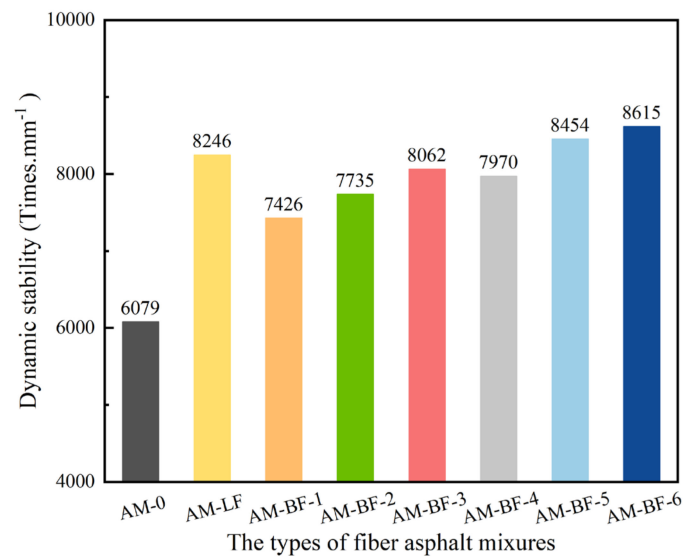


Figure 10. The results of rutting tests.

3.5.1. Rutting Resistance at a High Temperature

As shown in Figure 10, the addition of fibers could improve the high-temperature stability of asphalt mixtures, while AM-BF-6 demonstrated the most significant enhancement in high-temperature performance, with an increase of 41.7% compared to AM-0. After the surface modification of the fibers, the removal of some polar components enhanced the oil absorption capacity of the fibers and improved the interface compatibility with the asphalt; and the rough and porous surfaces were also more beneficial to the penetration and diffusion of the asphalt components. The interlocking effect between the modified bagasse fibers and asphalt was further strengthened, enhancing the overall structural strength and deformation resistance of the mixture. Additionally, surface modification also improved the thermal stability and mechanical properties of the fibers. All in all, regarding the ternary

composite modification, AM-BF-6 exhibited the highest dynamic stability, which was 4.5% higher than AM-LF.

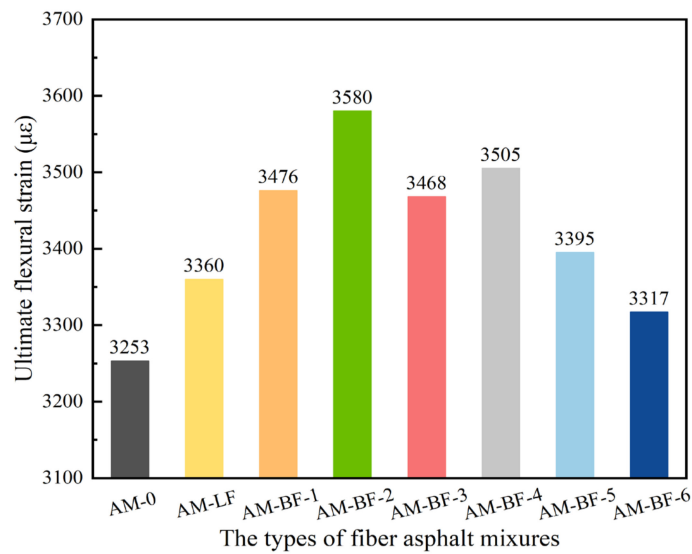


Figure 11. The results of bending tests at a low temperature.

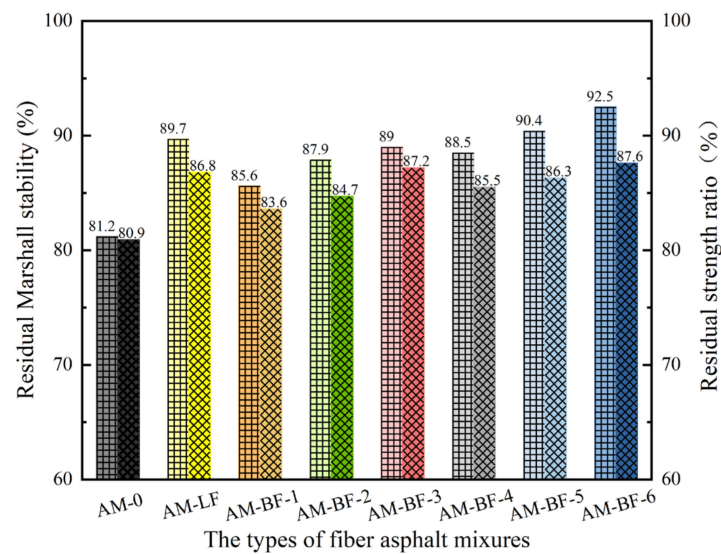


Figure 12. The results of water stability tests.

3.5.2. Cracking Resistance at a Low Temperature

As shown in Figure 11, it could be observed that the low-temperature performance of the asphalt mixtures was improved by bagasse fibers, while surface modification had no significant influence on the anti-cracking performance of the mixtures. Among the asphalt mixtures with bagasse fibers, AM-BF-2 showed the best low-temperature performance. After modification, the surface chemical structure, micropore distribution, and specific surface area of bagasse fibers changed partially, which facilitated the combination between the fibers and asphalt, enhancing the interfacial friction and load transfer capacity of the fibers. However, the binary and ternary composite modifications could cause a little damage to the structure of bagasse fibers, leading to a slight decrease in the low-temperature performance, like AM-BF-5 and AM-BF-6.

3.5.3. Water Stability

A water immersion Marshall test and a freeze–thaw splitting test were employed to evaluate the water stability of the asphalt mixtures. The residual Marshall stability and residual strength ratio of all the mixtures are shown in Figure 12. The left side of every histogram shows the residual Marshall stability, while the right side of every histogram shows the residual strength ratio. It could be confirmed that AM-BF-6 demonstrated the best water stability. As previously explained, due to the reduction in surface polar functional groups, removal of partial amorphous components, and enhancement of interfacial interactions, the modified fibers became more hydrophobic, which prevented water from permeating the interface between the asphalt and fibers and then decreased the expansion induced by freeze–thaw cycles and damages caused by water. In conclusion, the water stability of the asphalt mixtures with bagasse fibers by the ternary composite modification was better than that of the lignin fibers.

4. Conclusions and Future Trends

This paper observed the physical and chemical characteristics of treated and untreated bagasse fibers and analyzed the rheological properties of asphalt binders with and without various fibers. Subsequently, the performance of asphalt mixtures with fibers was evaluated. The following conclusions were obtained:

1. In accordance with the SEM images, it was verified that chemical modification could remove impurities on the surface of fibers, promote fibrillation, and make the fibers flexible. In addition, it was speculated that long-term heating may also damage the fiber structure and weaken the supporting function of the cell wall.
2. The result of FTIR revealed that sodium hydroxide had a significant impact on delignification, resulting in the presence of a cleaner cellulose phase with a high degree of polymerization, thus promoting the formation of a looser structure. Moreover, all the modification schemes could remove hydrophilic functional groups.
3. The result attained by the oil absorbing test showed that the five types of modified bagasse fibers exceed BF-1 regarding the value of the oil absorption ratio, which was caused by the loose structure of the fibers and partial removal of major components (i.e., cellulose, hemicellulose, and lignin). The increments were 15.0% for BF-2, 42.4% for BF-3, 31.6% for BF-4, 59.5% for BF-5, and 68.5% for BF-6.
4. In accordance with the DSR test, the asphalt binder with and without fibers, in terms of performance at a high temperature, ranked as follows: AB-BF-6 > AB-LF > AB-BF-5 > AB-BF-3 > AB-BF-4 > AB-BF-2 > AB-BF-1 > AB-0. The three-dimensional network comprised of fibers, and the SBS copolymer could hinder the fluidity of the asphalt. Meanwhile, the fibers could increase the stiffness of the asphalt binder by absorbing many asphalt components, enhancing the high-temperature deformation resistance of the asphalt binder, and the modification of fibers could also cause the promotion of comprehensive performance. The variation in the result of the BBR test was based on the same reason.
5. The road performance of the asphalt mixtures was significantly improved by bagasse fibers, confirmed by a series of comparative analyses. Modified bagasse fibers led to a much more significant enhancement in high-temperature performance compared to their impact on low-temperature performance. Furthermore, the ternary composite modification of bagasse fibers could effectively balance rutting resistance at a high temperature, cracking resistance at a low temperature, and the water stability of the asphalt mixtures. Overall, the performance of the asphalt mixtures with bagasse fibers by the ternary composite modification was close to that of lignin fibers.

In addition, the asphalt pavement was affected by complex factors, including loading, environment, and so on. The bonding mechanisms between the bagasse fibers and asphalt are a key issue that needs to be addressed for widespread applications of bagasse fibers. In the future, endeavors should be conducted to compare the performance of asphalt binders and asphalt mixtures with original bagasse fibers or modified bagasse fibers under

hygrothermal environmental conditions, respectively. Furthermore, it is necessary to verify the pavement performance of asphalt mixtures with bagasse fibers in practical pavement construction and observe their long-term road performance.

Author Contributions: H.X.: Conceptualization, Methodology, Project administration, Review, and Editing; Y.J.: Data curation, Formal analysis, and Writing—Original draft; C.Z.: Validation, Investigation, Resource, Review, and Editing; W.L.: Funding acquisition, Investigation, and Supervision; Z.L.: Supervision, Data curation, Review, and Editing; Z.H.: Validation, Review, and Editing. All authors have read and agreed to the published version of the manuscript.

Funding: This research was supported by the Natural Science Foundation of Guangxi (Grant NO. 2024GXNSFAA010308), Nanning Science and Technology Project (Grant NO. 20223039), Guangxi Science and Technology Project (Grant NO. ZY21195043), Shaanxi Technology Innovation Team (2024RS-CXTD-56), and Shaanxi Province “Scientists + Engineers” team construction (2023KXJ-281).

Data Availability Statement: Data are contained within the article.

Conflicts of Interest: Chunsheng Zhu was employed by the company Xinjiang Transportation Investment (Group) Co., Ltd. Weidong Liu was employed by the company Guangxi Key Laboratory of Road Structure and Materials, Guangxi Transportation Science and Technology Co., Ltd. The remaining authors declare that the research was conducted in the absence of any commercial or financial relationships that could be construed as a potential conflict of interest.

References

- Cai, M.; Peng, C.; Cheng, C. Study on the Rheological Properties of Formic Acid Lignin Modified Asphalt. *Buildings* **2023**, *13*, 655. [\[CrossRef\]](#)
- Li, Z.; Zhang, X.; Fa, C.; Zhang, Y.; Xiong, J.; Chen, H. Investigation on characteristics and properties of bagasse fibers: Performances of asphalt mixtures with bagasse fibers. *Constr. Build. Mater.* **2020**, *248*, 118648. [\[CrossRef\]](#)
- Li, J.; Luo, C.; Jie, J.; Cui, H. Rheological Properties and Microscopic Morphology Evaluation of UHMWPE-Modified Corn Stover Oil Bio-Asphalt. *Buildings* **2023**, *13*, 2167. [\[CrossRef\]](#)
- Safirzadeh, S.; Chorom, M.; Karimi, R.; Ariz, A.; Behravan, H.R.; Fadami, M. Effects of alkaline pretreatments on chemical composition of sugarcane bagasse for easy degradation in soil. *Sugar Tech* **2017**, *19*, 89–94. [\[CrossRef\]](#)
- Caro, S.; Vega, N.; Husserl, J.; Alvarez, A.E. Studying the impact of biomodifiers produced from agroindustrial wastes on asphalt binders. *Constr. Build. Mater.* **2016**, *126*, 369–380. [\[CrossRef\]](#)
- Bilba, K.; Arsène, M.-A.; Ouensanga, A. Sugar cane bagasse fibre reinforced cement composites. Part I. Influence of the botanical components of bagasse on the setting of bagasse/cement composite. *Cem. Concr. Compos.* **2003**, *25*, 91–96. [\[CrossRef\]](#)
- de Sá, L.R.V.; de Oliveira Faber, M.; da Silva, A.S.A.; Cammarota, M.C.; Ferreira-Leitão, V.S. Biohydrogen production using xylose or xylooligosaccharides derived from sugarcane bagasse obtained by hydrothermal and acid pretreatments. *Renew. Energy* **2020**, *146*, 2408–2415. [\[CrossRef\]](#)
- Cardona, C.; Quintero, J.; Paz, I. Production of bioethanol from sugarcane bagasse: Status and perspectives. *Bioresour. Technol.* **2010**, *101*, 4754–4766. [\[CrossRef\]](#)
- Bhardwaj, N.K.; Kaur, D.; Chaudhry, S.; Sharma, M.; Arya, S. Approaches for converting sugarcane trash, a promising agro residue, into pulp and paper using soda pulping and elemental chlorine-free bleaching. *J. Clean. Prod.* **2019**, *217*, 225–233. [\[CrossRef\]](#)
- Cabral, M.R.; Nakanishi, E.Y.; Dos Santos, V.; Palacios, J.H.; Godbout, S.; Savastano, H.; Fiorelli, J. Evaluation of pre-treatment efficiency on sugarcane bagasse fibers for the production of cement composites. *Arch. Civ. Mech. Eng.* **2018**, *18*, 1092–1102. [\[CrossRef\]](#)
- Ali, M.A.S.S.; Jimat, D.N.; Nawawi, W.M.F.W.; Sulaiman, S. Antibacterial, mechanical and thermal properties of PVA/starch composite film reinforced with cellulose nanofiber of sugarcane bagasse. *Arab. J. Sci. Eng.* **2022**, *47*, 5747–5754. [\[CrossRef\]](#)
- Mansor, S.; Zainuddin, N.; Aziz, N.; Razali, M.; Joohari, M. Sugarcane Bagasse Fiber—An Eco-Friendly Pavement of SMA. *AIP Conf. Proc.* **2018**, *2020*, 020032.
- Buritawaj, A.; Suddeepong, A.; Akkharawongwhatthana, K.; Horpibulsuk, S.; Yaowarat, T.; Hoy, M.; Arulrajah, A.; Rashid, A.S.A. Hemp fiber-modified asphalt concretes with reclaimed asphalt pavement for low-traffic roads. *Sustainability* **2023**, *15*, 6860. [\[CrossRef\]](#)
- Li, X.; Tabil, L.G.; Panigrahi, S. Chemical treatments of natural fiber for use in natural fiber-reinforced composites: A review. *J. Polym. Environ.* **2007**, *15*, 25–33. [\[CrossRef\]](#)
- Zhou, Y.; Fan, M.; Chen, L. Interface and bonding mechanisms of plant fibre composites: An overview. *Compos. Part B Eng.* **2016**, *101*, 31–45. [\[CrossRef\]](#)
- Sánchez, M.L.; Patino, W.; Cardenas, J. Physical-mechanical properties of bamboo fibers-reinforced biocomposites: Influence of surface treatment of fibers. *J. Build. Eng.* **2020**, *28*, 101058. [\[CrossRef\]](#)

17. Laluce, C.; Roldan, I.U.; Pecoraro, E.; Igbojonu, L.I.; Ribeiro, C.A. Effects of pretreatment applied to sugarcane bagasse on composition and morphology of cellulosic fractions. *Biomass Bioenergy* **2019**, *126*, 231–238. [[CrossRef](#)]
18. Seki, Y.; Kılınç, A.Ç.; Dalmis, R.; Atagür, M.; Köktaş, S.; Göktaş, A.A.; Çelik, E.; Seydibeyoğlu, M.Ö.; Önay, A.B. Surface modification of new cellulose fiber extracted from *Conium maculatum* plant: A comparative study. *Cellulose* **2018**, *25*, 3267–3280. [[CrossRef](#)]
19. Sepe, R.; Bollino, F.; Boccarusso, L.; Caputo, F. Influence of chemical treatments on mechanical properties of hemp fiber reinforced composites. *Compos. Part B Eng.* **2018**, *133*, 210–217. [[CrossRef](#)]
20. Chen, Z.; Chen, Z.; Yi, J.; Feng, D. Preparation method of corn stalk fiber material and its performance investigation in asphalt concrete. *Sustainability* **2019**, *11*, 4050. [[CrossRef](#)]
21. Ranganagowda, R.P.G.; Kamath, S.S.; Bennehalli, B.; Muddanna, A.; Sampathkumar, D.; Venkateshappa, S.C. Spectral studies on chemically modified single areca fibre. *Mater. Today Proc.* **2018**, *5*, 28018–28025. [[CrossRef](#)]
22. Sanjay, M.; Madhu, P.; Jawaid, M.; Senthamarai Kannan, P.; Senthil, S.; Pradeep, S. Characterization and properties of natural fiber polymer composites: A comprehensive review. *J. Clean. Prod.* **2018**, *172*, 566–581. [[CrossRef](#)]
23. Kalia, S.; Thakur, K.; Celli, A.; Kiechel, M.A.; Schauer, C.L. Surface modification of plant fibers using environment friendly methods for their application in polymer composites, textile industry and antimicrobial activities: A review. *J. Environ. Chem. Eng.* **2013**, *1*, 97–112. [[CrossRef](#)]
24. Chen, Z.; Liu, B.; Feng, D.; Li, G. Adsorption mechanism between corn stalk fiber and asphalt. *Sustainability* **2022**, *14*, 12863. [[CrossRef](#)]
25. Boumediri, H.; Bezazi, A.; Del Pino, G.G.; Haddad, A.; Scarpa, F.; Dufresne, A. Extraction and characterization of vascular bundle and fiber strand from date palm rachis as potential bio-reinforcement in composite. *Carbohydr. Polym.* **2019**, *222*, 114997. [[CrossRef](#)] [[PubMed](#)]
26. Moubarik, A.; Grimi, N.; Boussetta, N. Structural and thermal characterization of Moroccan sugar cane bagasse cellulose fibers and their applications as a reinforcing agent in low density polyethylene. *Compos. Part B Eng.* **2013**, *52*, 233–238. [[CrossRef](#)]
27. Qiang, X.; Lei, L.; Yi-jun, C. Study on the action effect of pavement straw composite fiber material in asphalt mixture. *Constr. Build. Mater.* **2013**, *43*, 293–299. [[CrossRef](#)]
28. Sheng, Y.; Zhang, B.; Yan, Y.; Li, H.; Chen, Z.; Chen, H. Laboratory investigation on the use of bamboo fiber in asphalt mixtures for enhanced performance. *Arab. J. Sci. Eng.* **2019**, *44*, 4629–4638. [[CrossRef](#)]
29. Wu, M.; Li, R.; Zhang, Y.; Wei, J.; Lv, Y.; Ding, X. Reinforcement effect of fiber and deoiled asphalt on high viscosity rubber/SBS modified asphalt mortar. *Pet. Sci.* **2014**, *11*, 454–459. [[CrossRef](#)]
30. Gao, J.; Wang, H.; Liu, C.; Ge, D.; You, Z.; Yu, M. High-temperature rheological behavior and fatigue performance of lignin modified asphalt binder. *Constr. Build. Mater.* **2020**, *230*, 117063. [[CrossRef](#)]
31. Bellatrache, Y.; Ziyani, L.; Dony, A.; Taki, M.; Haddadi, S. Effects of the addition of date palm fibers on the physical, rheological and thermal properties of bitumen. *Constr. Build. Mater.* **2020**, *239*, 117808. [[CrossRef](#)]
32. Chen, Z.; Yi, J.; Chen, Z.; Feng, D. Properties of asphalt binder modified by corn stalk fiber. *Constr. Build. Mater.* **2019**, *212*, 225–235. [[CrossRef](#)]
33. *ASTM D6114*; Standard Specification for Asphalt-Rubber Binder. ASTM International: West Conshohocken, PA, USA, 2023.
34. Ministry of Transport of the People's Republic of China. *JT/T533-2020: Fiber for Asphalt Pavements*; China Communication Press: Beijing, China, 2020.
35. *ASTM D7175-15*; Standard Test Method for Determining the Rheological Properties of Asphalt Binder Using a Dynamic Shear Rheometer. ASTM International: West Conshohocken, PA, USA, 2015.
36. *ASTM D6648-08*; Standard Test Method for Determining the Flexural Creep Stiffness of Asphalt Binder Using the Bending Beam Rheometer. ASTM International: West Conshohocken, PA, USA, 2008.

Disclaimer/Publisher's Note: The statements, opinions and data contained in all publications are solely those of the individual author(s) and contributor(s) and not of MDPI and/or the editor(s). MDPI and/or the editor(s) disclaim responsibility for any injury to people or property resulting from any ideas, methods, instructions or products referred to in the content.